20th Australasian Fluid Mechanics Conference
Perth, Australia
5-8 December 2016

# Local field effects on magnetic suppression of the converging Richtmyer-Meshkov instability

**V. Wheatley[1], W. Mostert[2], D. M. Bond[1] and R. Samtaney[3]**

[1]Centre for Hypersonics
University of Queensland, Brisbane, Queensland 4072, Australia

[2]Graduate Aerospace Laboratories
California Institute of Technology, Pasadena, California 91125, USA

[3]Mechanical Engineering, Physical Science & Engineering Division
King Abdullah University of Science and Technology, Thuwal 23955-6900, Saudi Arabia

**Abstract**

We examine how the suppression of the converging shock-driven Richtmyer-Meshkov instability by an applied magnetic field is dependent on the local magnetic field strength and orientation. In particular, we examine whether the extent of suppression can be reasonably predicted by a linear model for the planar case. This is done for cylindrically converging cases with a high perturbation wavenumber and two different initial magnetic field configurations.

## Introduction

The Richtmyer-Meshkov instability (RMI) of shock-accelerated density interfaces is highly detrimental to the chance of achieving a fusion burn in inertial confinement fusion (ICF) experiments [1]. In these experiments, a capsule containing fuel is imploded by a converging shock wave [2]. Conditions achieved at the centre of the implosion are sufficient to initiate fusion reactions, but a variety of factors including RMI-initiated mixing between the fuel and capsule material have thus far prevented a fusion burn from consuming all the fuel [2]. In these experiments, the materials involved are rapidly ionized. The interaction of such plasmas with magnetic fields can be approximated using ideal magnetohydrodynamics (MHD).

It has been demonstrated that the MHD RMI can be suppressed by the presence of a seed magnetic field in both planar [3, 4, 5, 6, 7] and converging geometries [8, 9]. In converging geometries - cylindrical and spherical implosions - the extent of RMI suppression is observed to be dependent on the local field orientation and strength, as can be seen in figure 1. This is due to the suppression mechanism being the transport of vorticity approximately parallel to the field by MHD waves [8]. In planar (2D, nonconverging) cases, it has been shown that the interface perturbation growth rate decays in the presence of a field normal to the interface [4, 5], and oscillates in the presence of a parallel field [6]. Magnetic fields of intermediate orientations produce a combination of these behaviors [7]. It is the converging cases, however, that are of current physical interest: axial seed magnetic fields have been applied in spherical ICF capsule implosion experiments, with demonstrated performance improvements [10], while the application of magnetic fields to cylindrical implosions is directly relevant to the magnetized liner inertial fusion (MagLIF) concept [11]. Developing optimal seed fields to maximize the performance of plasma implosions is complicated by their geometry and strength affecting the converging shock distortion [12] and strength [13], in addition to the nonuniform suppression of the RMI. The ability to rapidly predict the extent of RMI suppression at all interface locations for any seed field would aid this development.

A linearized model for the planar MHD RMI has been developed that predicts its behavior for arbitrary field conditions [7]. In this paper, we first derive an expression for the perturbation amplitude history from the model. We then examine how accurately using local field conditions in this expression predicts the variation of interface perturbaton behavior seen in the high wavenumber ($k$=128), cylindrically converging RMI cases shown in figure 1.

## Planar Model Interface Behavior

In [7], a model for the planar MHD RMI in the presence of an initial uniform magnetic field $\mathbf{B}_0 = (B_{0x},\ B_{0z})$ is derived by solving a linearized, incompressible, impulse driven initial value problem. The constant densities of the fluids below and above the interface are $\rho_1$ and $\rho_2$, respectively, the velocity imparted by the impulse in the $z$ (interface-normal) direction is $V$, and initial interface perturbation is $\eta_0 e^{ikx}$. The model provides an expression for the velocity perturbations normal to the interface of the form

$$w'(x,z,t) = \hat{w}(z,t)e^{ikx}, \tag{1}$$

where the mean interface location is $z = 0$. Assuming the interface amplitude $\eta(t)$ remains small ($\eta(t) \ll 2\pi/k$), to leading order it is given by

$$\eta(t) = \eta_0 + \int_0^t \hat{w}(0,\tau)d\tau. \tag{2}$$

Utilizing the expression for $\hat{w}$ from [7], we now carry out this integration to obtain

$$\begin{aligned}\eta(t) \quad = \quad & \eta_0 + K_\eta \left[ \frac{\theta+\bar{\alpha}_1}{\theta-\alpha_1} e^{\theta\tau} - \frac{\bar{\theta}+\bar{\alpha}_1}{\bar{\theta}-\alpha_1} e^{\bar{\theta}\tau} \right. \\ & \left. + K_2 \left( \frac{\theta+\alpha_2}{\theta(\theta-\alpha_1)} e^{\theta\tau} - \frac{\bar{\theta}+\alpha_2}{\bar{\theta}(\bar{\theta}-\alpha_1)} e^{\bar{\theta}\tau} \right) \right]_0^t, \end{aligned} \tag{3}$$

where

$$K_\eta = \frac{\eta_0 k V \mathcal{A}}{2i\omega},\ K_2 = \frac{-2B_{0z}k}{\sqrt{\rho_1}+\sqrt{\rho_2}} \sqrt{\frac{\rho_2}{\rho_1}}, \tag{4}$$

and this Atwood number is

$$\mathcal{A} = \frac{\rho_2 - \rho_1}{\rho_1 + \rho_2}. \tag{5}$$

The complex $\theta$ and $\alpha$ values in fluid $j$ are given by

$$\theta = \sigma + i\omega,\ \alpha_j = \alpha_{zj} + i\alpha_{xj}, \tag{6}$$

where

$$\alpha_{xj} = c_{Ajx}k,\ \alpha_{zj} = c_{Ajz}k, \tag{7}$$

$$\sigma = -B_{0z}k \frac{\sqrt{\rho_1}+\sqrt{\rho_2}}{\rho_1+\rho_2}, \tag{8}$$

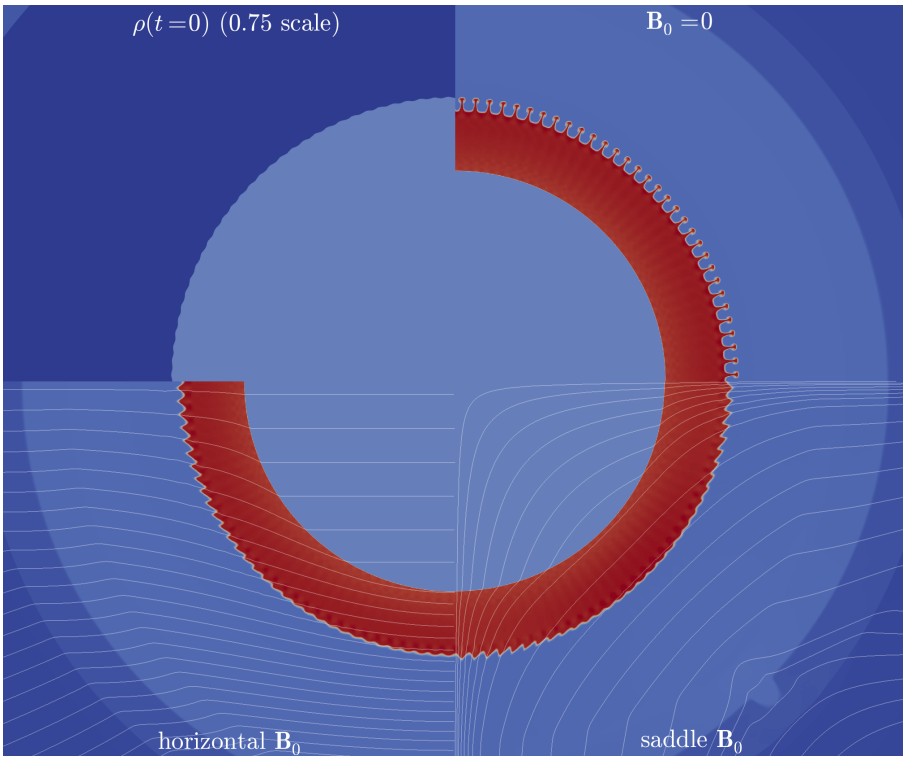


Figure 1: Initial ($t = 0$, top left) and evolved ($t = 0.8$) density distributions for simulations of the cylindrically converging RMI with three different initial magnetic fields: zero field (top right); a uniform horizontal field (bottom left, case C1); and a saddle field (bottom right, case C3). Field lines are shown where relevant. Generated from the simulations documented in [8].

$$\omega = k\left[\frac{2B_{0x}^2}{\rho_1+\rho_2} + \left(B_{0z}\frac{\sqrt{\rho_2}-\sqrt{\rho_1}}{\rho_1+\rho_2}\right)^2\right]^{1/2}. \tag{9}$$

Here, the Alfvén wave velocity in fluid $j$ is

$$\mathbf{c}_{Aj} = (c_{Ajx}, c_{Ajy}, c_{Ajz})^T = \frac{\mathbf{B}_0}{\sqrt{\rho_j}}. \tag{10}$$

From the above expressions, note that the decay of perturbation growth, governed by $\sigma$, is governed by the normal component of the magnetic field. Oscillations in the perturbation amplitude, at frequency $\omega$, are most strongly influenced by the field component parallel to the interface.

### Comparison to Local Interface Perturbation Behavior

To assess the accuracy of equation 3 in predicting the local, early-time perturbation behavior in the converging MHD RMI, we compare to the cylindrical simulations shown in figure 1, which are documented in [8]. Cylindrical cases were selected to simplify the analysis and interpretation. For high perturbation wavenumbers, the RMI has the opportunity to develop before the effects of convergence and the subsequent Rayleigh-Taylor instability (RTI) become dominant [9]. Thus we compare to the highest wavenumber cases ($k = 128$) presented in [8]. The initial magnetic field strength, characterized by $\beta = 2p_0/B_0^2 = 32$, is such that the interface perturbations still exhibit substantial growth, but the instability does not become highly nonlinear. Here, $p_0 = 1$ is the initial nondimensional pressure of the unshocked fluids. Two initial magnetic fields are investigated: a uniform horizontal field, denoted case C1; and a saddle-point field (see the lower right quadrant of figure 1), denoted case C3. The nondimensional initial densities in the simulations are $\rho_1 = 1$ outside the interface and $\rho_2 = 5$ within, resulting in an Atwood number of $\mathcal{A} = 2/3$. The converging shock that drives the instability is initialized via a cylindrical Riemann problem where the fluid outside of radius $r = 2$ has density $3\rho_1$ and pressure $12.1p_0$. This results in a shock Mach number of approximately 2.2 upon arrival at the initial interface radius $r = 1$. Finally, the initial perturbation amplitude is $\eta_0 = 2\pi/25k$. This initial condition is shown in the top left quadrant of figure 1.

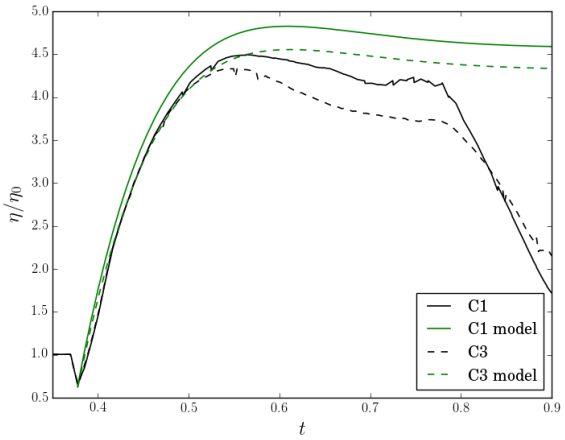


Figure 2: Comparison of model and computational interface amplitude histories where the local magnetic field orientation is approximately $\pi/6$ from the interface normal. These correspond to $\theta = \pi/16$ for the uniform field (C1) case and $\theta = \pi/32$ for the saddle field (C3) case.

Comparisons between the computational perturbation amplitude history and the model are made at azimuthal locations at angle $\theta$ to the horizontal in figures 2-5. For case C1, $\theta$ values of $\pi/16$, $3\pi/16$, $5\pi/16$ and $7\pi/16$ are investigated. At these az-

imuthal locations, the local field ranges from near perpendicular to near parallel to the interface. To study locations with similar local field angle in case C3, the C1 $\theta$ values are halved. As is conventional, post-shock values of parameters are used in the model [5].

Figure 2 shows perturbation behavior at locations where the local magnetic field is at an angle of approximately $\pi/6$ to the interface normal. Here, the model predicts a rapid decay of the initial growth rate combined with a long period, low amplitude oscillation. Prior to $t = 0.75$, the perturbation behavior in the converging simulations agrees remarkably well given the many potential sources of error: in addition to the planar model not accounting for the effects of compressibility, nonlinearity and flow convergence, it also assumes periodicity. This implies that the vorticity being transported from adjacent perturbations is identical to that for the one under consideration. In the cylindrical simulations, the magnetic field, and hence the vorticity transport, vary continuously around the interface. After $t = 0.75$, the Rayleigh-Taylor instability of the interface becomes dominant, driving down the perturbation amplitude as it begins to effect a phase inversion. This occurs after the growth of the RMI has saturated, leading to a convenient separation between the effects of the two instabilities. We note that the model accurately predicts both the level and timing of RMI growth saturation.

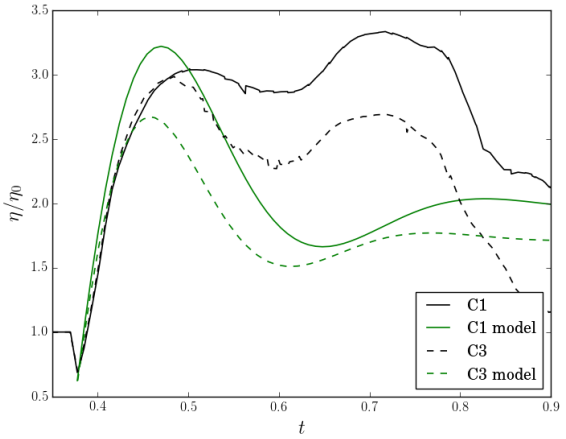


Figure 3: Comparison of model and computational interface amplitude histories where the local magnetic field is at an intermediate angle to the interface. These correspond to $\theta = 3\pi/16$ for the uniform field (C1) case and $\theta = 3\pi/32$ for the saddle field (C3) case.

Figure 3 compares the perturbation behavior at locations where the parallel component of the field has approximately double the magnitude of the normal component. Here, the model predicts the same rapid decay of the initial growth, followed by a higher-amplitude oscillation that is rapidly damped. The model successfully predicts the approximate magnitude and timing of the initial peak in the simulated perturbation amplitudes, but significantly overpredicts the amplitude of the oscillation, and hence underpredicts the perturbation amplitude at the end of the RMI dominated phase. The RTI again becomes dominant after $t = 0.75$.

Figure 4 illustrates the perturbation amplitude histories at locations where the parallel component of the field is significantly larger (approximately 4.5 times) than the normal component. After the brief initial growth phase, the model predicts a damped oscillation of the perturbation amplitude. The model has returned to being in good agreement with the behavior seen in the converging simulations, with both the initial peak in amplitude, the oscillation frequency and the rate of damping being reasonably well predicted. Owing to the slow damping of oscillations, there is no longer a clear separation between the RMI and RTI dominated phases.

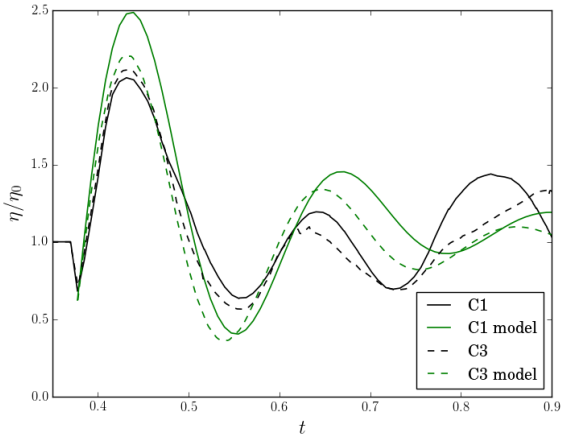


Figure 4: Comparison of model and computational interface amplitude histories where the local magnetic field is at an intermediate angle to the interface. These correspond to $\theta = 5\pi/16$ for the uniform field (C1) case and $\theta = 5\pi/32$ for the saddle field (C3) case.

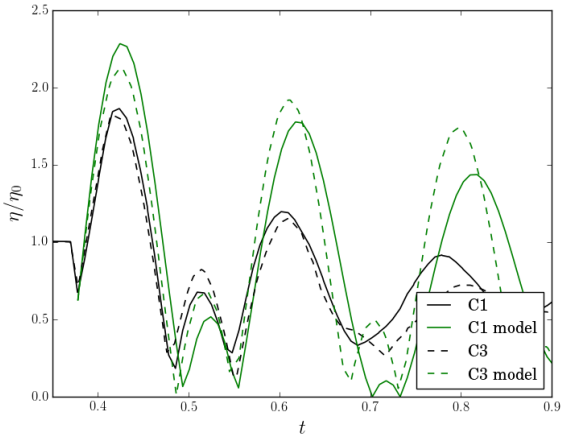


Figure 5: Comparison of model and computational interface amplitude histories where the local magnetic field is near parallel to the interface. These correspond to $\theta = 7\pi/16$ for the uniform field (C1) case and $\theta = 7\pi/32$ for the saddle field (C3) case.

Finally, perturbation behavior when the local field is near parallel to the interface is shown in figure 5. Note that we have actually plotted the magnitude of the perturbation amplitude, so slope discontinuities occur when the phase of the perturbations inverts. At this location, the model predicts a slowly damped oscillation of the perturbation amplitude. The model predicts both the peak amplitude and oscillation frequency seen in the cylindrical simulations reasonably well. The damping rate of the oscillations, however, is substantially greater in the simulations. As in the previous case, the oscillations triggered by the RMI have not subsided by the time of RTI onset, leading to the effects of the instabilities merging together at late times.

It is important to note that although the oscillations triggered by the RMI persist for longer as the angle between the magnetic field and the interface decreases, the extent of RMI suppression increases: both the peak and mean perturbation amplitude

decrease as the field becomes parallel to the interface. From figures 2-5, it is clear that the accuracy of model predictions is sensitive to the local magnetic field. Inaccuracies due to the effects of nonlinearity, compressibility and flow convergence are present at all locations. This suggests that the least accurate predictions (at $\theta = 3\pi/16$ for case C1 and $\theta = 3\pi/32$ for case C3) occur where the effects of non-periodic vorticity transport are strongest. In figure 1, it can be observed that the field line curvature at the interface is greatest close to these locations, which would enhance the non-uniformity of vorticity transport.

### Conclusions

An expression for the interface perturbation amplitude history in the planar MHD RMI has been derived from an existing linear, incompressible model. The capability of this model to predict the perturbation behavior in cylindrical shock-driven MHD RMI simulations was examined for a high perturbation wavenumber and two different magnetic field configurations. It was determined that the model provided reasonable estimates of the peak perturbation amplitude and the time this occurs at all locations investigated. The accuracy of predictions of perturbation behavior following the initial peak was found to dependent on the local magnetic field. Physically, it was seen that perturbation growth due to the RMI becomes more strongly suppressed as the magnetic field orientation approaches that of the interface. Around the majority of the interface, there is sufficient time for the RMI to saturate prior to the onset of the RTI dominated phase of the evolution.

### Acknowledgements

This research was supported by the KAUST Office of Sponsored Research under award URF/1/2162-01. V. Wheatley was supported an Australia Research Council Discovery Early Career Researcher Award (project number DE120102942).

### References

[1] J. D. Lindl, R. L. McCrory, and E. M. Campbell, Progress toward ignition and burn propagation in inertial confinement fusion, *Physics Today* **45**, 32 (1992).

[2] J. D. Lindl, O. Landen, J. Edwards, E. Moses, NIC Team, et al., Review of the national ignition campaign 2009-2012, *Phys. Plasmas*, **21**, 020501 (2014).

[3] R. Samtaney, Suppression of the Richtmyer-Meshkov instability in the presence of a magnetic field, *Phys. Fluids* **15**, L53 (2003).

[4] V. Wheatley, R. Samtaney, and D. I. Pullin, Stability of an impulsively accelerated perturbed density interface in incompressible MHD, *Phys. Rev. Letters*, **95**, 125002 (2005).

[5] V. Wheatley, R. Samtaney, and D. I. Pullin, The Richtmyer-Meshkov instability in magnetohydrodynamics, *Phys. Fluids* **21**, 082102 (2009).

[6] V. Wheatley, R. Samtaney, D. I. Pullin and R. M. Gehre, The transverse field Richtmyer-Meshkov instability in magnetohydrodynamics, *Phys. Fluids*, **26**, 016102 (2014).

[7] V. Wheatley, R. M. Gehre, R. Samtaney and D. I. Pullin, The Magnetohydrodynamic Richtmyer-Meshkov instability: The Oblique Field Case, *Proceedings of the 29th International Symposium on Shock Waves*, Springer, New York (2013).

[8] W. Mostert, V. Wheatley, R. Samtaney and D. I. Pullin, Effects of magnetic fields on magnetohydrodynamic cylindrical and spherical Richtmyer-Meshkov instability, *Phys. Fluids*, **27**, 104102 (2015).

[9] A. Bakhsh, S. Gao, R. Samtaney and V. Wheatley, Linear simulations of the cylindrical Richtmyer-Meshkov instability in magnetohydrodynamics, *Phys. Fluids*, **28**, 034106 (2016).

[10] M. Hohenberger, P.-Y. Chang, G. Fiskel, J. P. Knauer, R. Betti, F. J. Marshall, D. D. Meyerhofer, F. H. Séguin, and R. D. Petrasso, Inertial confinement fusion implosions with imposed magnetic field compression using the OMEGA Laser, *Phys. Plasmas* **19**, 056306 (2012)

[11] A. B. Sefkow, S. A. Slutz, J. M. Koning, M. M. Marinak, K. J. Peterson, D. B. Sinars and R. .A. Vesey, Design of magnetized liner inertial fusion experiments using the Z facility, *Phys. Plasmas*, **21**, 072711 (2014).

[12] W. Mostert, V. Wheatley, R. Samtaney and D. I. Pullin, Effects of seed magnetic fields on magnetohydrodynamic implosion structure and dynamics, *Phys. Fluids*, **26**, 126102 (2014).

[13] W. Mostert, D. I. Pullin, R. Samtaney and V. Wheatley, Converging cylindrical magnetohydrodynamic shock collapse onto a power-law-varying line current, *J. Fluid Mech.*, **793**, 414 (2016).